Vibration damping of marine lifting surfaces with resonant piezoelectric shunts

Laetitia Pernod, Boris Lossouarn, Jacques-André Astolfi, Jean-François Deü

Vibration Damping of Marine Lifting Surfaces with Resonant Piezoelectric Shunts

Laetitia Pernod[1,2], Boris Lossouarn[1,*], Jacques-André Astolfi[2], Jean-François Deü[1]

[1] Laboratoire de Mécanique des Structures et des Systèmes Couplées (LMSSC), Conservatoire national des arts et métiers (Cnam), 292 Rue Saint-Martin, 75003, Paris, France

[2] Institut de Recherche de l'Ecole Navale (IRENav), EA 3634 - Ecole Navale, 29240, Brest, France

* Corresponding author.
e-mail: boris.lossouarn@lecnam.net

Abstract

Marine lifting surfaces may undergo flow-induced vibrations due to fluid sources of excitation, leading to shorter life cycles due to structural fatigue and critical to the acoustic performances (*e.g* hydrofoil singing). As such, accurate understanding of the fluid-structure response of marine structures, as well as vibrations control and damping, are critical to many maritime applications. In particular, this work investigates the potential of the electromechanical coupling inherent to piezoelectric materials for passive vibration damping of a cantilever blunt flat plate under hydrodynamic flows. A prototype equipped with piezoelectric ceramics connected to an inductor, in order to act as a resonant piezoelectric shunt, is specifically designed for this study. Its flow-induced vibrations are first assessed within the water tunnel of IRENav to identify the natural frequency of interest to control. It shows that the plate is subjected to von Kármán vortex-shedding with two configurations, namely lock-off for the first-bending mode, and lock-in with the first torsional mode. The latter results in the most extreme vibration cases but is also the most difficult to control. Therefore, the first-bending mode is selected for this first experimental assessment. Second, semi-passive control strategies, using the resonant piezoelectric shunt, have been tested on the targeted natural frequency both in air and in still water. Subsequent comparisons show similar coupling factors, meaning that the performances of the resonant shunt should also be similar in air and in still water. Moreover, a numerical model, based on fluid-structure-piezoelectricity coupling, is also set-up to compute the coupling factors. Hence, a valuable numerical tool is provided for future designs of more complex geometries. Finally, experimental vibration mitigation is achieved both for still water and under hydrodynamic flows, experimentally proving the feasibility and relevance of this control solution for maritime applications.

Keywords: Flow-induced vibrations; Resonant piezoelectric shunt; Passive vibration damping

1. Introduction

Applications for marine lifting surfaces are progressively expanding and gaining economic importance in a growing number of maritime engineering fields. Marine lifting surfaces are indeed used as hydrofoils for high-speed ships, stabilizers, rudders, marine propellers and turbine blades. However, when subjected to hydrodynamic flows, these submerged structures may undergo strong fluid-structure interactions such as flow-induced vibrations, with almost always unwanted and harmful consequences. Indeed, flow-induced vibrations may trigger a sharp increase in the vibration amplitude when there is a coincidence between a natural frequency of the structure and a hydrodynamic excitation frequency [1, 2]. Such high-amplitude vibrations lead to shorter life cycles due to structural fatigue, and reduced acoustic discretion if the acoustic wave created by the structural vibrations have enough energy to travel to the far field. Therefore, vibrations control and damping solutions, as well as accurate understanding and prediction of the hydroelastic response of marine lifting surfaces, are critical to many maritime applications [3].

Because of their drastic consequences, flow-induced vibrations phenomena have been treated by a variety of engineering fields, from civil engineering to aeronautics, offshore, communications and marine propulsion. For instance, since the infamous collapse of the Tacoma bridge over the Narrows in 1940, bridges are now designed with consideration of the flow-induced vibrations. The world's tallest building, the Burj Dubai Tower, was purposely shaped to reduce the vortex-induced loads on the tower [4]. Oscillations of transmission lines, underwater cables, moored structures, pipelines and offshore risers, as well as galloping and flutter of aircraft control surfaces due to flow-induced forces were also extensively reported. More specifically for marine lifting surfaces, underwater sounds and vibrations of hydraulic machinery and propeller singing are also caused by a class of flow-induced vibrations [3]. Due to this diversity of flow-related vibrations, there exists a multitude of publications on that issue, scattered among a vast number of journals and books, with as many different descriptions and terminologies. In an attempt to provide a unified overview, Naudascher and Rockwell [5] propose a description of flow-induced vibrations in terms of their basic elements: body oscillators, fluid oscillators and sources of excitation. Sources of excitation are assessed for both the body and fluid oscillators, and classified in three categories, namely: i) extraneously-induced excitation caused by fluctuations in flow velocities of pressure that are independent of any flow instability originating from the structure considered, and independent of structural movements, ii) instability-induced excitation triggered by a flow-instability that is intrinsic to the flow system and therefore inherent to the flow created by the structure considered and iii) movement-induced excitation due to fluctuating forces arising from the movements of the vibrating body. For the present case study of a hydrofoil subjected to flow-induced vibrations under hydrodynamic flows, we shall mainly be concerned with extraneously-induced vibrations in the form of turbulence contained within the incoming flow (similar to a random excitation), and a particular class of instability-induced excitation, namely vortex-shedding from the blunt trailing edge (similar to a tonal excitation). Indeed, vortex-induced vibrations are considered to be a primary damage mechanism responsible for most sound, vibration and fatigue problems in hydraulic machinery and marine propulsion [6,7].

There are many different ways to control vibrations. Among them, piezoelectric devices are widely used for vibration control [8]. Piezoelectricity is the ability of a piezoelectric material to perform a two-way electro-mechanical conversion, either *via* the direct effect (*i.e* when pressured it generates an electrical charge), or *via* the inverse effect (*i.e* when placed in an electric field it strains mechanically). For vibration control applications, it is suitable to use man-made polycrystalline ceramic materials, that were processed to exhibit significant piezoelectric properties, such as lead zirconate titanate (PZT). However, classical PZT ceramics suffer from a brittle nature, so they cannot be easily attached to curved structures. To increase the strain limit, packaged PZT composites were developed by applying prestress through the surrounding layers [9–11]. This technique also offers the added benefit of an environmentally sealed packaging guarantying a protection from the surrounding fluid to the electric parts of these transducers. Thanks to all the aforementioned reasons, packaged PZT ceramics are one of the most used transducers for applications in submerged systems, in particular for modal analysis, vibration control, sound elimination and energy harvesting [11].

There are two main methods for vibration control using piezoelectricity: active vibration control and passive vibration control. Even though the former can be used to effectively reduce the vibrations of the structure [12–16], it has some limitations. Indeed, active control methods require a feedback control system including sensors, digital signal processors, power amplifiers, actuators and external electric sources, which is not very convenient in a confined submerged system. On the contrary, purely passive techniques are simple to implement and inherently stable. Passive reduction of structural vibration may be implemented with a shunted piezoelectric transducer, either *via* a simple resistor (*i.e* a resistive shunt) or *via* a resistor in series with an inductor (*i.e* a resonant shunt). Since the formulation of these shunts by Hagood and von Flotow in 1991 [17], much work has been performed on researching the optimal configurations for uni-modal damping [18–21], multi-modal damping [22,23], and designing inductors with high inductance values [24,25]. Vibration mitigation using piezoelectric shunts is thus a well-established and documented technique when used in air. Several authors also highlighted interesting features of these control solutions making them suitable candidates for an application in underwater sound absorption [26,27]. Moreover, Li et al. numerically investigated in [28] the feasibility of passive flutter control of flexible foils in various viscous fluids, using a piezoelectric circuit with an RL shunted PZT beam. However, to the exception of this numerical work, it seems that no other authors investigated the performance of a resonant piezoelectric shunt for vibration damping in still water, let alone under hydrodynamic flows.

This work investigates the potential of the electromechanical coupling inherent to piezoelectric materials for passive vibration damping of a simple hydrofoil under hydrodynamic flows. Principles of resonant piezoelectric shunt damping are recalled in Section 2. Section 3 then introduces the prototype, that is specifically designed for this study and represents a first experimental assessment of vibration mitigation using a resonant piezoelectric shunt under hydrodynamic flows. The hydrofoil is equipped with piezoelectric ceramics connected to an inductor in order to act as a resonant piezoelectric shunt. First, hydrodynamic tests have been performed in the IRENav water tunnel for various Reynolds numbers, in order to investigate its flow-induced vibrations (Section 4). Results show that the hydrofoil is subjected to von Kármán vortex shedding from its trailing edge. Moreover, there is a significant lock-in phenomenon between the von Kármán vortex shedding and the first torsional mode. These tests also highlight the natural frequency of interest to be controlled, that is the first bending mode in the present study. Second, control strategies, using the resonant piezoelectric shunt device, have been tested on this natural frequency. For this purpose, an experimental modal analysis in still air and in still water is carried out,

using two transducers as actuators to provide the excitation and two transducers for the piezoelectric shunt (Section 5). With this methodology, it is possible to determine the open- and short-circuit natural frequencies in order to compute the piezoelectric coupling factor. Indeed, the latter is related to the expected performance of the vibration damping strategy. Third, the values for the resistive and inductive components of the RL-shunt are inferred from the coupling factor and the natural frequencies. Fourth, these two configurations (coupling factors in still air and water) are compared to the numerical results obtained from a finite element model that is concurrently developed (Sections 6 & 7). Fifth, the control solution is tested in air and water in open and short circuits configurations (Section 8.1). Finally, in Section 8.2, vibration mitigation is achieved both for still water and under hydrodynamic flows, proving the feasibility and relevance of the control solution for maritime applications, such as hydrofoils or propellers. Limitations of the current study and work still undergoing are also highlighted.

2. Principle of Resonant Shunt Damping

Structural vibration damping may be obtained when shunting piezoelectric material with passive electrical circuits, such as the resonant piezoelectric shunt described by Hagood and von Flotow [17]. For instance, Fig. 1 shows a cantilever beam equipped with a piezoelectric transducer connected to a resonant shunt in order to mitigate the transverse vibrations. It consists in converting part of the vibratory mechanical energy into electrical energy, which is then dissipated through a resistance R. Moreover, it is possible to create an electrical resonance with the addition of an inductance L to the electrical circuit, which involves the piezoelectric capacitance. The inductance L and the resistance R are considered in series, as shown on Fig. 1. When this electric resonance matches one of the natural frequencies of the structure, the energy transfer between the mechanical and electrical domains is increased. As a consequence, a passive resonant piezoelectric shunt behaves similarly to a tuned mass-damper [24]. Once the shunt is correctly tuned, the performances of this vibration damping solution are only dependent on a modal coupling factor k_c defined using the natural frequencies of the system for two different electrical conditions [18]: (i) the short-circuit condition and (ii) the open-circuit condition. The former corresponds to zero voltage across the piezoelectric transducer (natural angular frequency ω_{sc}), while the latter corresponds to zero electric charge displacement within the circuit (natural angular frequency ω_{oc}). The coupling factor k_c is inferred from these two electrical conditions using:

$$k_c = \sqrt{\frac{{\omega_{oc}}^2 - {\omega_{sc}}^2}{{\omega_{sc}}^2}} \tag{1}$$

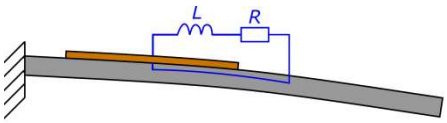

Fig. 1. Cantilever beam with a piezoelectric transducer (featured in light brown) connected to a resonant shunt (blue electrical circuit).

Moreover, once the coupling factor k_c is known, optimal vibration mitigation exists using a passive resonant piezoelectric shunt, corresponding to optimal inductance:

$$L = \frac{1}{C{\omega_{oc}}^2} \tag{2}$$

and resistance values:

$$R = \sqrt{\frac{3}{2}}\frac{k_c}{C\omega_{oc}} \tag{3}$$

derived from a minimization of a transfer function involving the mechanical displacement to control [18], where C is the blocked capacitance, corresponding to the piezoelectric capacitance measured when preventing displacement of the mechanical system.

Around the mechanical resonance, the continuous structure in Fig. 1 may be approximated by a one-degree-of-freedom spring-mass system. Hence, the electromechanical coupling may be represented by the following model, corresponding to the balance law of mechanical forces, and one electrical equation, associated with the balance of electric charges on the piezoelectric electrodes [18,24] :

$$M\ddot{U} + K(1 + k_c^2)U = k_c\sqrt{\frac{K}{C}}q + F \tag{4}$$

$$L\ddot{q} + R\dot{q} + \frac{1}{C}q = k_c\sqrt{\frac{K}{C}}U \tag{5}$$

where U is the displacement of the mass M, K the stiffness in short-circuit condition, q the electric charge displacement and F represents the forcing term corresponding to the load applied to the structure. In case of hydrodynamic loads, these are dependent on the nature of the flow (laminar or turbulent) as well as the nature of the fluid-structure interactions [5], and will be discussed further in Section 4, relatively to the specific case considered in this paper.

3. Experimental Setup

3.1 Geometry and Materials of the Structure

The structure considered in this work is shown on Fig. 2a: it is an aluminium flat plate consisting of a rectangular platform of 191 mm × 100 mm × 6 mm (length, width, thickness) and a rectangular extension of 80 mm × 31 mm × 10 mm at its base, whose purpose is to clamp the structure to the tunnel wall. The latter extends outside of the tunnel test section, and thus is not in contact with the water. Hence, the effective length for the fluid numerical model is 191 mm, corresponding to the wetted surface, while the length for the structure numerical model is 271 mm in order to account for the added weight and stiffness of the extension (for details relative to the numerical models, refer to Section 7). Furthermore, two rectangular cavities of dimensions 61.5 mm × 71 mm × 1 mm are machined on both sides of the plate to insert two piezoelectric transducers on each side (Fig. 2b). Indeed, embedding the transducers in the structure rather than gluing them on top of the surface avoids creating added thickness and local roughness, which may cause added turbulence or flow detachment if the roughness size is in the order of the boundary layer thickness [29]. The piezoelectric transducers are bonded to the plate surface using a vacuum bagging method with an epoxy adhesive. Then, a thin layer of paraffin is added on top of the transducers to fill the residual depth of the cavity and reconstruct the surface so that it is level to the plate surface. Channels are also machined in the plate and the extension root to allow the passage of electric wires from the electrodes (two on each patch) to the components of the electrical control circuit (*i.e* the shunt).

The piezoelectric transducers are P-876.A15 DuraAct patches commercialized by PI Ceramic and consist of a PIC-255 active layer sandwiched between two soft thin encapsulating Kapton shell layers, as presented on the schematic in Fig. 3a. The packaging is used to apply prestress to the active layer in order to avoid cracks, thus increasing the allowable curvature radius of the PZT ceramics [9–11]. As a consequence, they can be glued more easily to curved surfaces. This last point is of particular interest for this application, as the objective is to move to hydrofoils, once the potential of the considered control solution has been assessed on the flat plate. Moreover, this environmentally sealed packaging guarantees a protection from the surrounding fluid to the electric parts of these transducers. Overall dimensions of the transducers (*i.e* including the encapsulating material) are 61 mm × 35 mm × 0.8 mm, while the encapsulated active layer is 50 mm × 30 mm × 0.5 mm (Fig. 3b). Material properties of the active layer are presented in a strain-charge form in Table 1 while the properties of the Kapton shell are summed up in Table 2, along with the properties of the aluminium used for the plate.

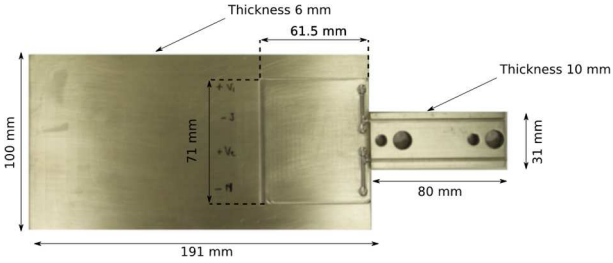

(a)

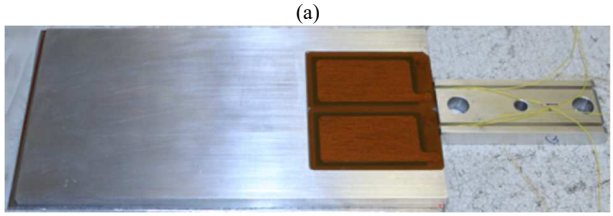

(b)

Fig. 2. (a) Geometry and dimensions of the aluminium flat plate featuring the cavity for the piezoelectric transducers and (b) Piezoelectric transducers glued on the flat plate.

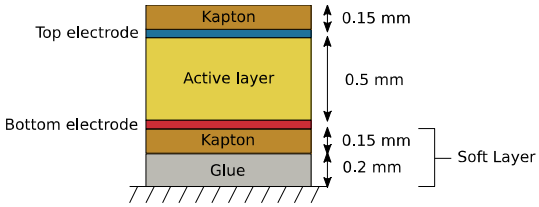

(a)

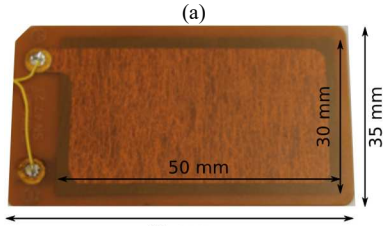

(b)

Fig. 3. (a) Schematic of a P-876.A15 patch, showing the active layer sandwiched between two soft thin encapsulating layers and (b) Geometry and dimensions of the encapsulated piezoelectric transducers.

Table 1: Material properties of the PIC-255 active layer in strain-charge form.

Coefficient	Units	Value
Density	kg/m^3	7800
Compliance matrix		
S_{11}^E	m^2/N	1.606×10^{-11}
S_{12}^E	m^2/N	-5.685×10^{-12}
S_{13}^E	m^2/N	-7.454×10^{-12}
S_{33}^E	m^2/N	1.909×10^{-11}
S_{44}^E	m^2/N	4.699×10^{-11}
S_{55}^E	m^2/N	4.699×10^{-11}
S_{66}^E	m^2/N	5.350×10^{-11}
Dielectric constants		
d_{31}	m/V	-1.867×10^{-10}
d_{33}	m/V	3.996×10^{-10}
d_{35}	m/V	6.174×10^{-10}
Relative permittivity		
ϵ_{11}^σ		1852
ϵ_{22}^σ		1852
ϵ_{33}^σ		1751

Table 2: Material properties of the aluminium plate and Kapton shell.

Coefficient	Units	Value
Aluminium		
Density	kg/m^3	2650
Tensile modulus	GPa	70
Poisson's ratio		0.33
Kapton shell		
Density	kg/m^3	1420
Tensile modulus	GPa	2.8
Poisson's ratio		0.3

3.2 Experimental Facility, Test Setup and Sensors

Experiments were carried out in the hydrodynamic tunnel at the Institut de Recherche de l'Ecole Navale (IRENav) of the French Naval Academy in France. The tunnel test section is 1 m long with a 192 mm square section. Available operational velocities in the test section range from 0.5 to 12 m/s and the effective velocity within the test section is induced from the pressure difference upstream and downstream of the inlet (refer to pressure sensors featured on Fig. 4). Finally, a honeycomb grid upstream of the test section allows for a 2% free stream turbulent intensity at the mid-section. For additional information about the hydrodynamic tunnel refer to [30].

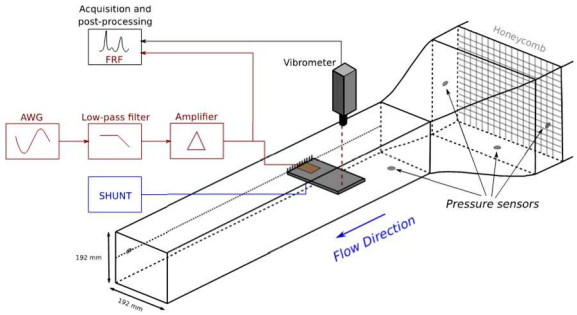

Fig. 4. Experimental test setup.

Vibration damping of the flat plate equipped with its four piezoelectric transducers is performed both (i) in air, (ii) completely submerged in still water and (iii) under hydrodynamic flows. For this purpose, the structure (a 100 mm chord length and 191 mm spanwise length) is mounted horizontally in a cantilever configuration within the hydrodynamic tunnel (Fig. 4). Moreover, the small tip clearance between the tip of the plate and the tunnel wall (1 mm) leads to minimal distortion of the flow and structure excitation due to the 3D effects of the tip vortex which cannot fully develop.

Vibrations measurements of the plate are carried out using a Doppler laser vibrometer located above the plate at a single point, located at the tip of the plate, on the leading edge as shown on Fig. 4. The laser vibrometer is a PDV-100. In this study it is set-up to provide non-contact vibrational velocity measurement in the 500 Hz frequency range. Two issues should be treated with care while measuring the structural response in water using a laser vibrometer. First, it is of prime importance to check and maintain the perpendicularity of the laser to the surface, in order to avoid parasitic reflection and refraction. Second, residual air bubbles may be present within the water (for instance when initiating the flow) and may trigger a parasitic response in the signal if crossing the laser's path. Results presented in this paper were obtained with these two points in check.

4. Flow-Induced Vibrations

Prior to assessing the potential of vibration damping of submerged structures using a resonant piezoelectric shunt, a preliminary study of the flow-induced vibrations of the structure is first carried out. There are two main objectives for this preliminary study. First, it characterizes the nature of both the excitation and vibrations due to the fluid loading. This helps understanding the potential benefits that vibration mitigation could have on this structure, and also highlights the frequency range that would be the most interesting to investigate. The latter corresponds to the second objective of this preliminary study. Indeed, as detailed in Section 2, the design choices of the electrical circuit (inductor and resistor) are guided by the value of the frequency to be controlled.

For this preliminary study, the structure is placed in water at an incidence of 0º and subjected to incident flow velocities ranging from 0.6 to 6 m/s, corresponding to Reynolds numbers from 6×10^4 to 6×10^5, while maintaining the pressure at subcavitating flows. Fig. 5a shows the vibration spectra of the plate for the range of incident velocities considered. The first two natural frequencies of the plate are visible for respective values of f_1 = 26.4 Hz and f_2 = 174.1 Hz. The spectra also exhibit additional components with a strong dependence to the Reynolds number: the local maximum close to 50 Hz for a Reynolds number of 1.5×10^5 is progressively shifted towards the high frequencies when increasing the Reynolds number. This phenomenon is characteristic of a vortex shedding process associated to von Kármán alleyways [1,2,5,6,30]: the boundary layer is developing on both sides of the plate but meets with a singularity at the trailing edge. The boundary layer then starts to shed alternatively from both sides of the plate, leading to the formation of a vortex street in the turbulent wake, first observed by Strouhal in 1878, while he was studying the relationship between the frequency of excitation and the wind velocity [31]. Mallock in 1907 [32] and Bénard in 1908 [33] then took the first modern pictures of the vortex street, featuring the alternating arrangement of vortices in the wake. This alternate shedding causes a periodic fluctuation of the hydrodynamic loads applied on the plate and is thus a source of excitation associated to a von Kármán shedding frequency f_{vk}. In the present case, a strong fluid-structure interaction between the second mode of the structure (corresponding to the 1st torsional mode)

and the shedding frequencies may be observed when their respective values coincide (around 174 Hz). This strong fluid-structure interaction is characterized by a sharp increase of the vibration amplitude.

Fig. 5b presents the corresponding Reynolds-Frequency diagram, which clearly highlights the linear evolution of the hydrodynamic excitation frequency with the Reynolds number. This linear evolution is given by:

$$S_t = \frac{f_{vk} e}{U_0} \tag{6}$$

with a constant Strouhal number S_t close to 0.2 when vortex shedding occurs (e is the plate thickness and U_0 the incident velocity) [5,6,31].

In the present case the Strouhal number is about constant to 0.194, confirming the existence of vortex shedding. However, for some Reynolds numbers between 4×10^5 and 6×10^5 the shedding frequencies no longer follow Strouhal's law, but instead keep a constant value of 174 Hz, despite the increase in the number of Reynolds. This is the phenomenon of frequency lock-in around the first mode of torsion: von Kármán's turbulent wake no longer evolves with its own dynamics but instead is organized around the natural frequency of the structure [5,34]. As a consequence, the strong fluid-structure interaction previously mentioned corresponds to this lock-in phenomenon.

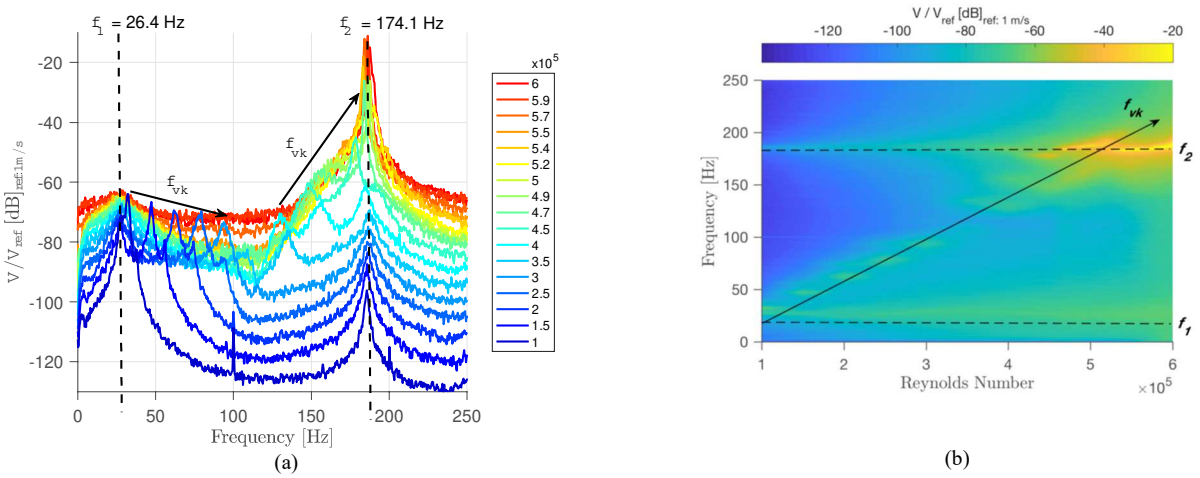

(a) (b)

Fig. 5. (a) Vibration spectra under hydrodynamic flows for different Reynolds numbers and (b) Corresponding Reynolds-frequency diagram. f_1 and f_2 are the first two natural frequencies and f_{vk} corresponds to the von Kármán shedding frequency.

Another important result of this preliminary study concerns the fluctuations of the natural frequencies to the Reynolds number (*i.e* to the flow velocity): Fig. 5a shows very little fluctuations for the first two natural frequencies. Therefore, the natural frequency of the plate may be considered quasi-constant to the flow velocity.

Finally, this preliminary study shows that the excitation provided by the fluid sources may be represented as the sum of a random, wide bandwidth component and of a tonal component. The former is due to the turbulence contained within the boundary layer flow, while the latter is due to von Kármán vortex-shedding and experiences a frequency shift related to the Reynolds number [6]. The most severe load cases are when the tonal component is close to a natural frequency of the structure and strong-coupling through lock-in may occur. In the present study, this particularly happens for the first torsional mode, so it would ideally be the most interesting mode to control. However, it is also the most difficult case, as there are complex interactions between different physical phenomena. As a consequence, in this research we chose a step-by-step methodology with an incremental difficulty, so the efficiency of the control solution is first assessed on the first bending mode, that is without clear lock-in of the von Kármán.

Since only the first bending mode is considered, a one degree-of-freedom approximation may be used [35], where the displacement U in equation (6) is the transverse motion of the plate. Furthermore, the fluid loading F in this case may be approximated as the sum of (i) the turbulence contained within the incoming flow and the boundary layer and (ii) a harmonic (or tonal) component linearly dependent on the flow velocity (Strouhal's Law) due to the vortex-shedding in a lock-off mode [5,6].

5. Methodology and Experimental Techniques

As seen in Section 2, in order to design the resonant shunt (made of an optimal inductance and a resistance), one needs to accurately determine the short- and open-circuit natural angular frequencies (ω_{sc} and ω_{oc}).

5.1 Design of the Resonant Shunt: Methodology

The most classical method to obtain the short- and open-circuit natural frequencies is to perform a modal analysis of the system in both electrical conditions. However, there are two main drawbacks when performing modal analysis on submerged structures.

First, it can be particularly difficult to perform modal analysis of submerged structures using classical force actuators (such as impact hammer or shaker), as (i) these structures are many times inaccessible, sometimes confined in small sealed spaces and (ii) the electronics of the sensors need to be protected from the surrounding water. Therefore, piezoelectric actuators have been classically used as exciters in modal analysis of submerged structures, due to their relatively small size and light weight compared to other electromechanical actuators [11,36]. For instance, several authors [29,37,38] tested and validated the use of embedded piezoelectric patches for mechanical excitation of hydrofoils under dynamic flows. Similarly, the two piezoelectric transducers on the trailing edge (TE) are used as actuators to provide the excitation while performing modal analysis of the plate, while the other two piezoelectric transducers (*i.e* on the leading edge – LE) are either used (i) in short-circuit or (ii) in open-circuit. The two piezoelectric transducers used as actuators are themselves excited using a group of three electrical components chained together in series to provide a broad-band excitation (noise signal): an arbitrary waveform generator (AWG), a low-pass filter and two amplifiers (refer to Fig. 4). This signal is used as an input for the acquisition and post-processing program. Since the vibrations of the plate are also monitored thanks to the Doppler laser vibrometer, the final output is the transfer function between the displacement and the applied voltage (m/V). Details concerning the manufacturer and product version for each of the specifics components used to provide the excitation are given in Table 3, along with the specifics of the sensors.

Table 3 : Details of the sensors and devices used to generate the excitation in still water

Device	Manufacturer	Product
Doppler laser vibrometer	Polytech	PDV 100
AWG	Hewlett-Packard	33120 A
Low-pass filter	NF Corporation	FV – 628 B
Amplifier 1	Bruel & Kjaer	2706
Amplifier 2	CRC	242 B

The parameters L and R of the shunt under hydrodynamic flows are assumed to be similar to that in still water, allowing to carry out modal analysis solely in the latter configuration. As stated in the previous section, Fig. 5a shows that the natural frequencies are quasi-constant to the flow velocities, so this assumption is perfectly legit in the present case. In addition, the coupling factors and shunt parameters in still water were derived for two transducers intended for vibration control (the other two being used as actuators), so a higher performance of the control solution should be obtained with the use of four transducers under hydrodynamic flows. Actually, moving from two to four transducers (i) doubles the modal fraction of strain energy, which controls the ability of every mode of vibration to concentrate the strain energy into the transducer element, resulting in a multiplication of the coupling factor by $\sqrt{2}$ (for more details, refer to Preumont et al., 2008 [39]) and (ii) doubles the capacitance of the shunt. Consequently, the inductance L is divided by 2.

Hence, the complete methodology used to design the resonant shunt under hydrodynamic flows may be summed up as:

1. Modal analysis of the plate under still water in short- and open-circuit conditions, using two transducers as actuators and two transducers in control;
2. Derivation of the two transducers - resonant shunt parameters (inductance L and resistance R) in still water from Eq. (2) and Eq. (3);
3. Since the natural frequencies are quasi-constant to the flow velocity (Section 4), the parameters of the two transducers - resonant shunt under hydrodynamic flows are the same as in still water;
4. To increase the performance of the damping solution, a four transducers shunt is used under hydrodynamic flows. Its design is made by multiplying the coupling factor by $\sqrt{2}$ and doubling the capacitance relatively to the two transducers shunt, resulting also in dividing the inductance by 2.

Finally, the different configurations that were tested in this work are summed up in Table 4.

Table 4: Configurations tested

Test n°	Medium	Configurations
1	Air without flow	• short-circuit: ω_{sc} • open-circuit: ω_{oc} • shunt on first bending mode • 2 transducers used as actuators • 2 transducers used for control
2	Water without flow	• short-circuit: ω_{sc} • open-circuit: ω_{oc} • shunt on first bending mode • 2 transducers used as actuators • 2 transducers used for control
3	Hydrodynamic flows	• velocities from 0.5 to 6 m/s • assumption: the shunt parameters are identical to still water • shunt on first bending mode • excitation provided by the flow • 4 transducers used for control

5.2 Modal Parameters and Damping Coefficients

Fig. 6 presents the experimental frequency response function in air and in still water using the two piezoelectric transducers on the trailing edge as actuators to provide the excitation. Note that these experiments were not directly realized within the hydrodynamic tunnel described in Section 3.2 but in a smaller cavity filled with water because there is no need for hydrodynamic flow at this point. However, the experimental setup, sensors and methodology are identical. These results are referred to as "the first experimental set" in the following. Table 5 sums up the characteristics of the first bending and first torsional modes in terms of natural frequencies in short- and open-circuits, coupling factors k_c and damping factors ξ. However, concerning the first torsional mode, it is difficult to clearly distinguishes between the short- and open- natural frequencies (identical in still water and even reversed in air, with an open-circuit natural frequency that seems lower than the short-circuit natural frequency). Actually, the electromechanical coupling is too low for the first torsional mode to determine coupling factors and natural frequencies for different electrical conditions. Notwithstanding, this does not call into question the value of the natural frequency for the first torsional mode, which is around 310.4 Hz, and the following observations and results, as this paper is focused on the first bending mode (refer to Section 4). Significant added mass effects are observed: the natural frequencies in air are reduced by around 50% in still water (more precisely, $f_{air}/f_{water} = 2.11$ for the first bending mode and 1.67 for the first torsional mode). This reduction may be explained by the inertial effects of the fluid on the structure (*i.e* the classical added mass effect), since the mass number is not small compared to unity ($M_a = \rho_f/\rho_s = 0.38$) [40].

Moreover, the coupling factors are similar in air and in still water, in particular for the first bending mode. This result is particularly important, as it demonstrates that the electro-mechanical coupling, critical for the good performances of the control solution, is not deteriorated by the immersion of the structure in a heavy fluid. This actually proves that vibration mitigation under hydrodynamic flows using a resonant piezoelectric shunt is *a priori* feasible, which is, to the best of the authors knowledge, the first time it has been experimentally demonstrated. However, the initial damping of the system is increased in still water so, even if possible, it will be harder to have a strong impact on vibrations. Indeed, the performances of the shunt are only functions of the piezoelectric coupling factor and the structural damping factor of the targeted mode [18]. As the added damping provided by the resonant shunt will be of proportionally lower importance relatively to the initial damping, it will have a lower effect. Last, coupling factors in Table 5 were determined for a two-transducers resonant shunt; therefore the coupling factors for a four-transducers resonant shunt may be estimated as 8.5% in air and 10% in still water for the first bending mode.

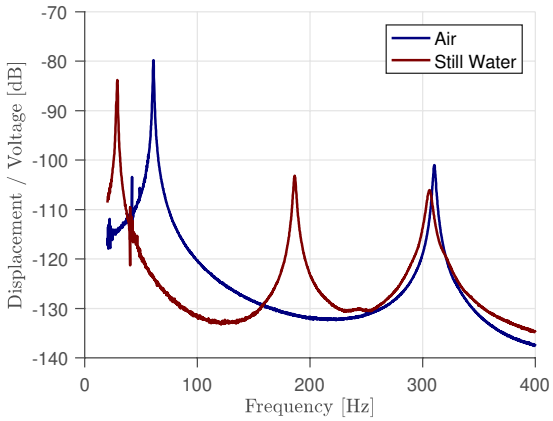

Fig. 6. In-air and in-water frequency response functions of the cantilever plate.

Table 5: Characteristics of the first bending and first torsional modes in air and in still water.

Medium	f_{sc} [Hz]	f_{oc} [Hz]	k_c [%]	ξ_{sc} [%]	ξ_{oc} [%]
First bending mode					
Air	60.99	61.10	6.04	0.75	0.76
Still water	28.87	28.94	7.08	1.65	1.56
First torsional mode					
Air	310.4	310.3		0.41	0.42
Still water	186.4	186.4		0.68	0.67

5.3 Technological Realization: Synthetic Inductor

The prime concern is to design and manufacture an appropriate resonant shunt device to mitigate the vibrations of the prototype. Table 6 presents the inductor values required to design a suitable resonant piezoelectric shunt for the configurations in air and in still water, inferred from the natural frequencies in open-circuit of Table 5 and the piezoelectric capacitance (64 nF for two transducers in parallel), according to Eq. (2). This application requires large inductance values (5 H < L < 500 H), which is one of the main drawbacks of the resonant shunt technique, since such high values may be difficult to obtain using passive inductors. Actually, the standard inductor series are usually limited to 0.5 H, which definitely cannot satisfy our application. This phenomenon is amplified by the low frequency range to control, requiring even higher values. The following two solutions may be used: i) a synthetic inductor or ii) custom designs and specific techniques to manufacture high inductance value components [24].

The first solution consists in building an active electronic circuit, made of one or more operational amplifiers and a number of passive resistors and capacitors, to mimics the electrical impedance of an inductor. High-values inductance may be synthesized using this approach. Moreover, this solution has the advantage of flexibility, as the synthesized inductance can easily be modified. In the present application, it means that control of the different configurations may be attempted using only one electronic circuit, instead of manufacturing one passive inductor for each of the configuration. The synthetic inductor used for this application is made from the Antoniou's circuit, modified by Senani to compensate for internal resistance, and is described in full details, with the relevant figures, in ref [18]. However, this solution is no longer a purely passive technique, but a semi-passive method because it requires a power supply. Furthermore, standard operational amplifiers cannot handle the high-voltage and low-current conditions typically required by piezoelectric materials, so specific circuits must sometimes be used [41].

For the scope of this paper, a resonant piezoelectric shunt is used, made using a synthetic inductor, easier to realize, in order to "pre-tune" the inductance values and check the vibration damping in water.

Table 6: Required inductance and resistance values for resonant piezoelectric shunt damping.

Medium	L [H]	R [Ω]
First bending mode		
Air	106	3.01×10^3
Still water	473	7.43×10^3

6. Mathematical Formulation

6.1 Governing Equations

A finite element model is used to solve the fluid-structure-piezoelectricy coupled multiphysics problem of the submerged cantilever plate equipped with piezoelectric transducers, described in Section 3. The problem is written in the frequency domain, under the assumption of an "acoustic" fluid, that is a compressible inviscid fluid. The governing equations are the Cauchy equation of motion for the mechanical part:

$$-\rho_s \omega^2 u_i = \sigma_{ij,j} \tag{7}$$

the Maxwell-Gauss equation in a dielectric medium for the electrostatic part:

$$D_{i,i} = 0 \tag{8}$$

and the Helmholtz equation for the fluid acoustic part (see *e.g* [42]):

$$-\frac{1}{\rho_f} p_{,ii} - \frac{\omega^2 p}{\rho_f c^2} = 0 \tag{9}$$

In equations (7) to (9), ρ_s and ρ_f are respectively the solid density and fluid density. First-order tensor $\boldsymbol{u}$ and second-order tensor $\boldsymbol{\sigma}$ are the displacement field and the Cauchy stress tensor relative to the structure. First-order tensor $\boldsymbol{D}$ is the electric displacement field, ω is the angular frequency used to solve the problem in the frequency domain and c is the celerity of sound in the fluid. Finally, p is the pressure fluctuation in the scattered field formulation of the fluid acoustic problem.

6.2 Closure with Constitutive Equations

The governing equations (7) to (9) of the coupled problem are partially closed using, on the one hand, the constitutive equation of a linear elastic material (Hooke's law) for the aluminium part:

$$\sigma_{ij} = C_{ijkl} \varepsilon_{kl} \tag{10}$$

and, on the other hand, the constitutive equations of piezoelectricity for the transducers:

$$\begin{cases} \varepsilon_{ij} = S^E_{ijkl} \sigma_{kl} + d_{kij} E_k \\ D_i = d_{ikl} \varepsilon_{kl} + \epsilon^{\sigma}_{ik} E_k \end{cases} \tag{11}$$

In equations (10) and (11), $\boldsymbol{\varepsilon}$ is the strain tensor, $\boldsymbol{C}$ is the fourth-order elasticity tensor, $\boldsymbol{S^E}$ is the fourth-order compliance tensor, $\boldsymbol{E}$ is the electric field, $\boldsymbol{d}$ is the third-order piezoelectric tensor and $\boldsymbol{\epsilon^{\sigma}}$ is the dielectric permittivity second-order tensor. Table 1 gives the values of the components of the piezoelectric coefficients in equation (11) using the Voigt notation.

6.3 Closure with Gradients Relationships

The governing equations (7) to (9) of the coupled problem are also closed using the gradient relationships written under the assumption of no geometric nonlinearities:

$$\varepsilon_{ij} = \frac{1}{2}\left[u_{i,j} + u_{j,i}\right] \tag{12}$$

and expressing the Maxwell-Faraday static equation (*i.e*. the electric field is curl-free and thus derives from an electric potential ϕ):

$$E_i = -\phi_{,i} \tag{13}$$

6.4 Coupling Conditions

To couple the three subdomains of the problem, the structural displacement $\boldsymbol{u}$, stress $\boldsymbol{\sigma}$ and strain $\boldsymbol{\varepsilon}$ fields are solved using Navier's equations (7), (10) and (12) while the electric field $\boldsymbol{E}$, electric displacement field $\boldsymbol{D}$ and the potential distribution Φ are solved using the electrostatics and piezoelectricity equations (8), (11) and (13), and the pressure p is solved using

Helmholtz equation (9), along with the two following coupling conditions: (i) the normal acceleration of the fluid is imposed by the vibration of the structure at the wetted wall, which is expressed by:

$$\frac{1}{\rho_f} p_{,i} n_i = \omega^2 n_i u_i \tag{14}$$

and (ii) the fluid imposes pressure forces at the interface with the structure, according to:

$$F_i = p n_i \tag{15}$$

6.5 Boundary Conditions

In addition to equations (7) to (15), several boundary conditions are considered. First, a fixed boundary ($\boldsymbol{u} = \boldsymbol{0}$) is imposed on part of the extension root (refer to Fig. 7) and sound hard boundaries (*i.e* fixed walls, $p_{,ii} n_i = 0$) are imposed on all the faces of the fluid domain, except on the top face where a free-surface ($p = 0$) condition is used. Finally, different electrical conditions are considered. Concerning the transducers used in control, when in short-circuit, all the electrodes are affected with an electrical ground condition ($\Phi = 0$), while in open-circuit half the electrodes are kept at the ground condition while the others are affected with an equipotential condition (Φ is constant, $\iint D_i n_i dS = 0$ on the surface of the electrode). Concerning the transducers used to provide the excitation, all the electrodes are affected with the ground condition when performing a modal analysis and with a harmonic electrical potential of amplitude ϕ_0 ($\phi(t) = \phi_0 e^{i\omega t}$) when performing a frequency response analysis.

7. Numerical Model

Design of a resonant piezoelectric shunt for vibration mitigation requires the determination of coupling factors. However, performing an experimental assessment of the coupling factors for each modification of the structure during the design stage is both extremely time consuming and expensive. To tackle this issue, it is of high interest to develop a numerical tool that can efficiently compute coupling factors, even for complex geometries. The objectives of this section are thus to (i) prove the feasibility of a numerical estimate of the coupling factors for a submerged structure, that is, using a fluid-structure-piezoelectricity coupling,(ii) assess the capability of the commercial code COMSOL Multiphysics to provide the tools for such a study and (iii) study the influence of the soft layer modelling on the coupling factors.

7.1 Structure modelling: general considerations

The structure is modelled using the “Finite Elements Structural Mechanics” module of the commercial code COMSOL Multiphysics. As stated in the presentation of the experimental setup (refer to Section 3.1), the effective structural length of the prototype for the structure model includes both (i) the wetted surface (the 191 mm × 100 mm × 6 mm rectangular platform) and (ii) the rectangular extension (80 mm × 31 mm × 10 mm) needed to clamp the structure to the tunnel wall (refer to Fig. 7a). Indeed, this extra material generates added mass and stiffness to the structural properties. Moreover, the channels machined in the plate to allow for the passage of electrical cables are also taken into account. As a point of fact, these channels are very close to the fixed boundary, so their influence on the overall stiffness of the structure is not negligible. This effect is again amplified by the fact that the fixed boundary does not run on all the width of the plate, but is very localized (see for instance Fig. 7a and Fig. 7b). Finally, to accurately predict the coupling factors due to the electromechanical coupling, it is necessary to include a soft layer below the active layer [20] when modelling the piezoelectric transducers (Fig. 7c). This soft layer is used as a medium to represent the combined contributions of the glue and of the encapsulating Kapton shell, as was presented on Fig. 3a.

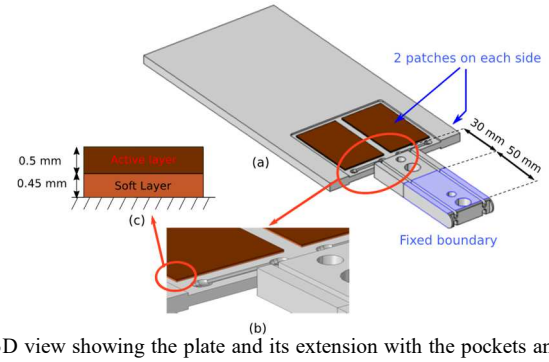

Fig. 7. Model of the plate: (a) global 3D view showing the plate and its extension with the pockets and channels, the piezoelectric transducers and the fixed boundary, (b) close-up on the root with details of the channels and modelling of the transducers and (c) bigger close-up on the transducers modelling, including the soft layer and active layer.

Hence, the main parameters of this numerical model are the following:

- Mesh type and cells size: mesh convergence on the natural frequencies and coupling factor is required for proper computing;
- Modelling of the clamping condition: length of the extension root over which a fixed boundary condition is used. Indeed, in the water tunnel, the clamping tail (*i.e* the extension root) is caught in a vice that is not perfectly rigid, and thus is difficult to accurately model. This is taken into account in the numerical model by adjusting the length of the extension root over which a fixed boundary condition is used, to match the experimental natural frequency of the first bending mode in air. For instance, Fig. 7a shows the fixed boundary in light blue, adjusted to 50 mm over the 80 mm of the extension root;
- Modelling of the soft layer: the presence of a soft layer (glue + encapsulating Kapton shell) between the active material of the piezoelectric transducer and the plate, decreases the level of electromechanical coupling because of stiffness loss. However, the actual thickness of the soft layer in the experimental setup is not accurately known (uncertainty on the thickness of the glue layer). Therefore, an equivalent soft layer thickness is adjusted to match the experimental coupling factor of the first bending mode.

The following subsections describe in full details the steps required to define the above parameters. Note that at this point, all the numerical data are adjusted relative to the second experimental set, that is the experiments within the hydrodynamic tunnel (contrary to the first experimental set realized in a smaller cavity filled with water and presented in Section 5 and Table 5).

7.2 Mesh convergence

Mesh convergence is realized on the first two natural frequencies (first bending and first torsional modes), both for short- and open-circuit conditions, as well as on their corresponding coupling factors k_{c1} and k_{c2}. Computations are carried out in air, using four transducers in control. The mesh is constituted of tetrahedral elements using quadratic serendipity shape functions, with different levels of refinement close to the fixed boundary, on the transducers and on the channels, as shown on Fig. 8. Because it is impossible to setup all parameters using one set of computations, assumptions are made on the other two parameters:

1) The fixed boundary is set-up as an ideal clamping condition over the whole length of the extension;
2) Computations for mesh convergence are realized with an *a priori* value of the soft layer, based on geometrical and empirical considerations. On the one hand, the thickness of the Kapton shell layer is 0.15 mm (manufacturer data), the total thickness of the transducer is 0.8 mm (manufacturer data), and the depth of the cavity is 1 mm (conception of the prototype). On the other hand, experimental observations reveal that the top of the transducer is level with the top of the cavity once the glue was added, meaning that the glue is approximately filling the residual space of the cavity, that is 0.2 mm (1 – 0.8 mm). Hence, an initial educated guess for the thickness of the soft layer is 0.2 (glue) + 0.15 (Kapton shell) = 0.35 mm. Materials for the piezoelectric transducers are defined to correspond to the manufacturer data (refer to Table 1), while materials for the aluminium plate and soft layer corresponds to classical aluminium and Kapton shell properties (refer to Table 2).

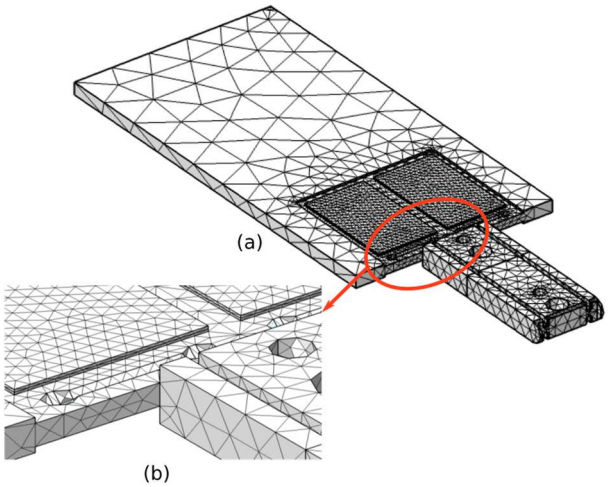

Fig. 8. Structural mesh (a) global 3D view and (b) close-up showing the different refinements close to the fixed boundary, on the transducers and on the channels.

Fig. 9a presents the results of mesh convergence in short-circuit for the first bending mode f_{sc1} and the first torsional mode f_{sc2}, while Fig. 9b presents the results of mesh convergence on the coupling factors. A great number of elements (348,200) is required to reach convergence, which can be explained by the presence of the channels close to the fixed boundary: because their effect is not negligible, they must be accurately modelled, requiring lots of small elements (refer to Fig. 8). However, to lower computation time and memory resources, a mesh with a lower level of convergence and fewer elements is suitable: a final structural mesh of 171,290 elements, corresponding to convergence levels of 5% on the first bending mode (natural frequency and coupling factor) and 1% for the first torsional mode, is used for subsequent computations (refer to the red dashed-line on Fig. 9).

Note: First, coupling factors for this simulation may seem inconsistent with the experimental values presented in Table 5 (12.5% vs. 6.04% for the first bending mode in air). Several reasons cause this impression: (i) as mentioned in the previous subsections, computations are compared to the second set of experiments, and not the first set. The values to be compared should therefore be 12.5% (numeric) to 10.6% (experiments) for four transducers. The remaining difference between 12.5% and 10.6% is due to (ii) the boundary condition on the clamping is not adjusted (ideal clamping in the numerical model) and (iii) the soft layer, representing the influence of the glue and encapsulating material, is also not yet properly adjusted (initial guessed value). Second, for the same reasons, the coupling factor for the first torsional mode may still be computed. Nonetheless, it's very low value (around 2.5%) confirms that the electromechanical coupling is very low for this mode (refer to Section 5).

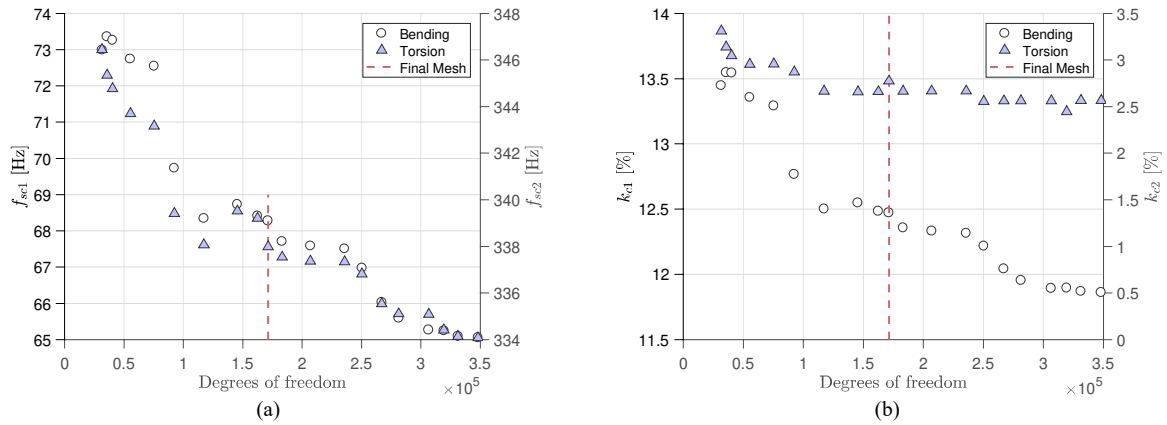

Fig. 9. Structural mesh convergence on (a) in-air natural frequencies and (b) corresponding coupling factors.

7.3 Clamping condition and soft layer modelling

Once a suitable converged mesh is selected, assumption 1) on the length of the fixed boundary layer is corrected. The clamping condition is indeed adjusted on the natural frequency of the first bending mode in air for two transducers: 61.60 Hz for the experimental results (coupling factor 7.66%), and 61.64 Hz for the numerical modelling (coupling factor 8.16%). The final length of the fixed boundary is 50 mm over the 80 mm of the extension. Then, assumption 2) on the soft layer thickness is adjusted from the initial guess of 0.35 mm, corresponding to a coupling factor k_{c1} of 8.16%, to 0.45 mm, corresponding to a coupling factor k_{c1} of 7.62% (better matching the experimental value in the hydrodynamic tunnel in air of 7.66%.). Table 7 sums up the methodology used to setup the numerical model, with the different sets of computations and their associated assumptions.

Table 7: Methodology used to setup the numerical model

Set of Computations	Conditions and Assumptions	Objective	Criteria / Results
1	• In air, four transducers • Different mesh configurations • Ideal clamping • Initial guess for the thickness of the soft layer	Mesh convergence	Convergence levels: • 5% for the 1st bending mode • 1% for the 1st torsional mode
2	• In air, two transducers • Converged mesh (171,290 elements) • Different clamping lengths • Initial guess for the thickness of the soft layer	Definition of clamping condition	Adjustment on the natural frequency of the 1st bending mode: • 61.60 Hz experimental • 61.64 Hz numerical
3	• In air, two transducers • Converged mesh (171,290 elements) • Adjusted clamping length (50 mm) • Initial guess for the thickness of the soft layer	Definition of soft layer modelling	Adjustment on the coupling factor of the 1st bending mode: • 7.66 % experimental • 7.62 % numerical
4	• In still water, two transducers • Converged mesh (171,290 elements) • Adjusted clamping length (50 mm) • Adjusted thickness of the soft layer (0.45 mm)	Fluid modelling	Numerical prediction of the coupling factor of the 1st bending mode: • 6.97 % experimental • 7.61 % numerical

7.4 Fluid modelling

For numerical analysis in still water, an additional acoustic fluid medium surrounding the structure is added, as shown on Fig. 10. The fluid domain is also meshed using quadratic tetrahedral elements with Lagrange shape functions, such that structural and fluid elements are compatible at the fluid-structure interface. Consequently, it is possible to compute the natural frequencies and coupling factors of the submerged structure for different configurations (such as position, shape, size and thickness of the piezoelectric transducers). For instance, Fig. 11 shows the mode shapes, natural frequencies and coupling factors (first bending mode only) computed using this numerical model, compared to the experimental results of the second experimental set in still water. It shows that, even though the adjustment of the numerical model was carried out in air for simplicity, there is a good agreement between the numerical and experimental results in still water, as the coupling factor of the first bending mode is overestimated by 3.5%. Concerning the natural frequencies, a greater error on the first torsional mode should be expected, as the adjustments of the numerical model parameters (clamping condition and soft layer thickness) were realized on the first bending mode in air.

This numerical model is thus very suitable and convenient to inform the design of the control solution for a given geometry. This is of high interest, since the numerical model may now be used to estimate the coupling factors when the four transducers are used for control, which is difficult to measure experimentally without another source of excitation. Moreover, in this particular case, numerical simulations are faster and less expensive than experimental testing. As a consequence, a validated numerical model is a highly valuable tool for the optimal conception of the prototype. An optimization algorithm on the transducers' positioning to maximize the coupling factors might even be added to the numerical model for further improvement of the design procedure.

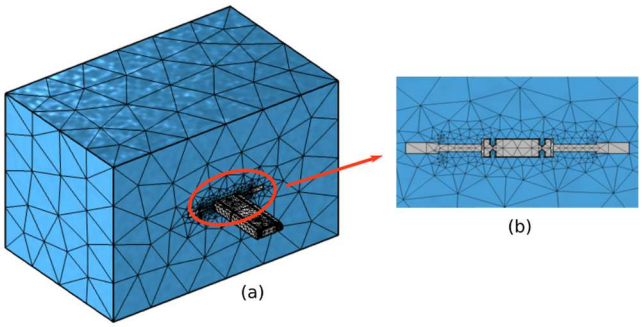

Fig. 10. Meshed acoustic fluid medium surrounding the structure for numerical analysis in still water

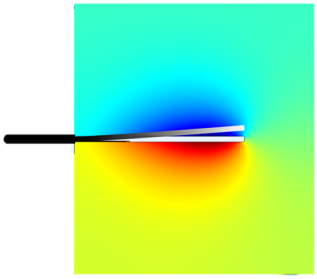

f_{exp} = 25.71 Hz
f_{num} = 26.61 Hz
$k_{c,exp}$ = 6.97 %
$k_{c,num}$ = 7.61 %
(a)

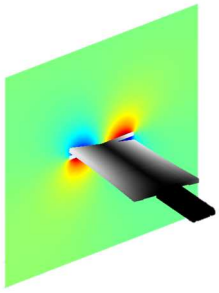

f_{exp} = 180.86 Hz
f_{num} = 170.75 Hz
(b)

Fig. 11. Numerical mode shapes for still water with their associated natural frequencies and coupling factors compared to experimental results for (a) the first bending mode and (b) the first torsional mode. The colormap represents the pressure field within the fluid, while the gray shades represent the displacement field on the structure, from the numerical simulations.

8. Experimental Vibration Damping

In the previous sections we proved, both experimentally and numerically, the *a priori* feasibility of vibration damping in water using a resonant piezoelectric shunt, as the coupling factors are similar to those in air. Moreover, we identified two technical solutions to realize the inductor, either through a synthetic inductor, or through a purely passive inductor capable of high-inductance values. We now assess the performances of the resonant shunt on the first bending mode of our prototype using the synthetic inductor, first in-air and in still water, then under different hydrodynamic flows.

8.1 In-air and in-still water vibration mitigation

Fig. 12a shows the experimental vibration mitigation of the first bending mode using the resonant piezoelectric shunt in air, and Fig. 12b in still water. As explained in the previous sections, in particular in Section 2, the resonant piezoelectric shunt is designed using equations (2) and (3). These equations correspond to the theoretical derivation of L, from the blocked capacitance C. However, for the experiments, a slightly different value of C should be used for accurate tuning of the resonant shunt [22,25]. For this purpose, a first estimate of the capacitance is obtained *via* direct measurement of the capacitance of one transducer glued to the plate. It is assumed that this measured capacitance is close enough to the blocked capacitance to derive a first value of the inductance L from equations (2) and (3). Then, manual tuning of the inductance L is realised according to the shape of the FRF of the response, to get equal peaks. This manual tuning is realised both in air and in water, as the coupling factor differs slightly (but not that much, as shown in Section 5.2: 6.04% in air and 7.08% in still-water).

Both frequency response functions exhibit the characteristic shape of a resonant shunt damping and visible vibration reduction. It also confirms that even though the coupling factors are similar, the reduction of the vibration amplitude provided by the control solution is lower in still-water, due to the added damping before control (refer to subsection 5.2). However, this is not the maximum of vibration reduction that could be provided using this control solution, as the resistance value was not yet optimized, due to limitations of the electric circuit. This is particularly true for the case in still water, for which the performances may be improved with a finer tuning of the resistance. But at present, optimal tuning of the shunt in still water is not an issue. Indeed, this set of experiments mainly aims to demonstrate that a resonant piezoelectric shunt also works as a tuned-mass-damper for vibration mitigation in water, which is proved by the existence of a local minimum on the controlled

frequency response functions. Moreover, only two of the four transducers were used in control (the other two being used for the excitation), so the performances will be increased when moving to four transducers.

These results are used as a reference for the design of the resonant shunt under hydrodynamic flows: the coupling factor in still-water is multiplied by $\sqrt{2}$ to estimate the coupling factor with four transducers used in control, then Eq. (2) and Eq. (3) are used to design the resonant shunt (also refer to subsection 5.1).

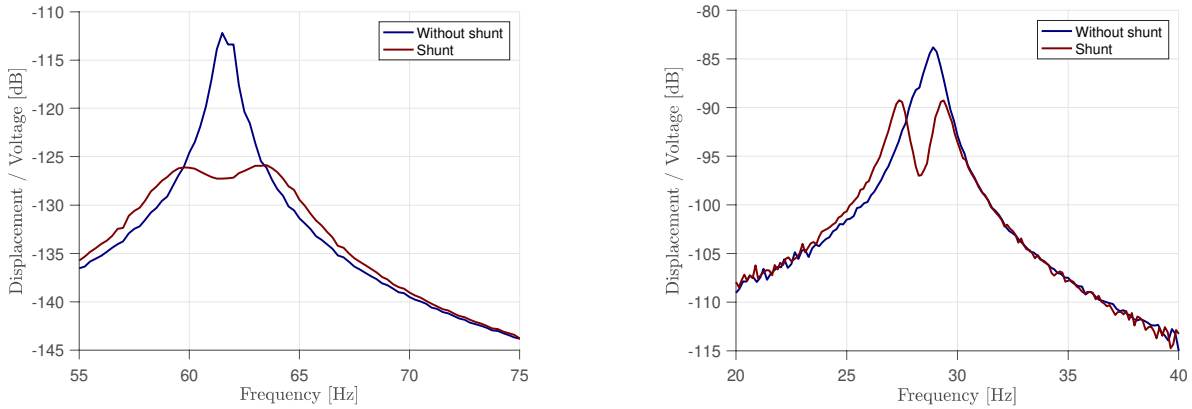

Fig. 12. Vibration damping of the first bending mode using a synthetic inductor in (a) air and (b) still water

8.2 Vibration damping under hydrodynamic flows

The next step is to assess the performances of the control solution under hydrodynamic flows, using four transducers for the resonant shunt. Fig. 13 presents the RMS (Root-Mean-Square) values of the tip velocity signal for different Reynolds numbers (*i.e* incoming flow velocities), without control and using the resonant shunt on the first bending mode. Vibration damping is observed, in particular for the velocities corresponding to a von Kármán shedding frequency f_{vk} close to the natural frequency of the prototype. Indeed, as presented in Section 4, the Strouhal number associated to vortex shedding is 0.194 for this prototype, and the maximum vibration mitigation is obtained for a Reynolds number of 84,000, that is an incoming velocity of 0.84 m/s (Fig. 13). Eq. (6) gives a shedding frequency of 27 Hz associated to these conditions, which is close to the natural frequency of the first bending mode in still water (25.71 Hz, refer to Section 7.4 and Fig. 11). The location for the maximum vibration reduction may be explained by the relationship between the shedding frequency and the overall damping of the system (that is the structure and the surrounding fluid). According to Blake et al, 1977 and Reese, 2010, [1,43], there is a strong relation between the damping of the system and the shedding frequency, as follows:

- When the shedding frequency is below a natural frequency of the structure, the mode is excited at a moderate amount and damped only by mechanical and sound mechanisms;
- When the shedding frequency is very close to a natural frequency, the mode is excited strongly with very little damping. There is a sharp increase in the amplitude of vibration because of this virtual loss of damping due to energy input from the surrounding flow. In some cases, lock-in may even occur (for instance, this is the case for the 1st torsional mode of the prototype, refer to Section 4);
- When the shedding frequency is above the natural frequency, the mode is weakly excited and is highly damped by additional hydrodynamic damping, which increases with flow velocity. In the present case, we can indeed observe a strong decrease of the vibration amplitude past a Reynolds number of 84,000.

Concerning the results in Fig. 13, note that the incoming flow is not completely stationary, so the results are slightly dependent on the duration of the testing. This probably explains some unexpected amplitudes in the uncontrolled case around a Reynolds number of 74,000. A more accurate analysis could be performed with more data points and a longer testing time.

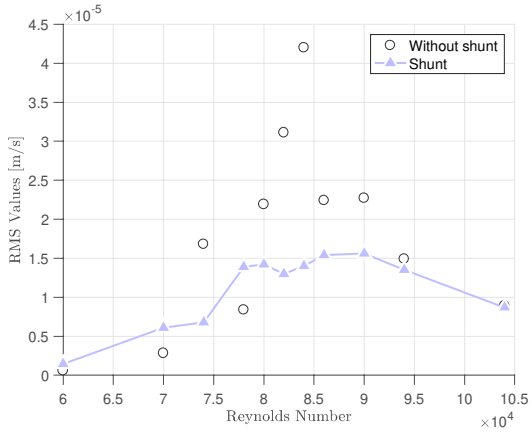

Fig. 13. Vibration damping of the first bending mode under hydrodynamic flows in terms of reduction of the Root Mean Square values of the temporal velocity signal

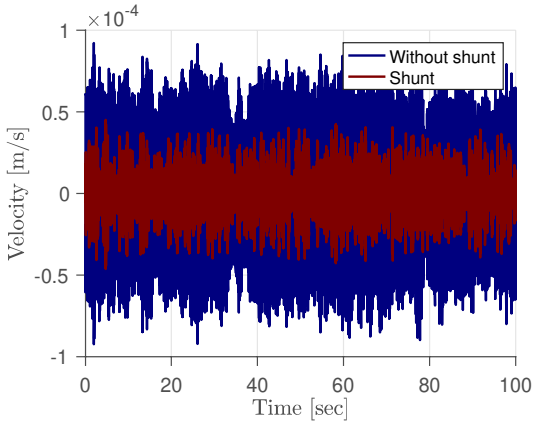

Fig. 14. Vibration damping of the first bending mode under hydrodynamic flows for a Reynolds number of 84,000.

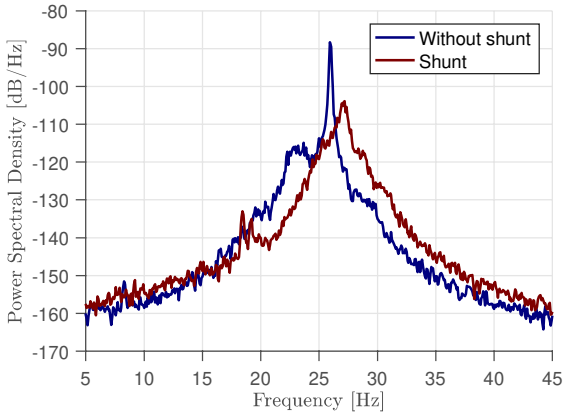

Fig. 15. Power spectral density for a Reynolds number of 84,000, with and without control of the vibrations.

Looking at time signals, Fig. 14 shows the velocity signals without control and using the resonant shunt for the condition with maximum reduction, that is a Reynolds number of 84,000 where the RMS value is reduced by a factor 3. Corresponding power spectral density is shown on Fig. 15, emphasizing the strong effect of the shunt on the vibrations (reduction of 15.6 dB/Hz). This is an important result, which proves that vibration damping using a resonant piezoelectric shunt under hydrodynamic flows is a functional solution for vibration mitigation around a structural resonance.

9. Conclusion and Further Work

This study constitutes a first experimental assessment of a resonant piezoelectric shunt for vibration mitigation under hydrodynamic flows. For this purpose, a prototype of a cantilever blunt flat plate subjected to von Kármán trailing-edge vortex shedding is specifically designed and manufactured to test the potential of the electromechanical coupling inherent to piezoelectric materials for passive vibration damping under hydrodynamic flows. The hydrofoil is equipped with four piezoelectric ceramics connected to an inductor, in order to act as a resonant piezoelectric shunt.

First, hydrodynamic tests have been performed in the IRENav water tunnel for various Reynolds numbers, in order to investigate its flow-induced vibrations. Results showed a strong fluid-structure interaction phenomenon between the natural frequencies of the structure and the hydrodynamic excitation frequencies due to von Kármán vortex shedding in the turbulent wake. In particular, the hydrodynamic excitation frequencies present a linear dependence to the Reynolds number, with a constant Strouhal of 0.194, to the exception of a frequency lock-in around the first torsional mode (around 174 Hz). These tests also highlight that the phenomenon of lock-in on the first torsional mode leads to the most extreme vibrations. However, for a first assessment of the control strategy with steps of incremental difficulty, the first bending mode with a lock-off situation is identified as the frequency to be controlled.

Second, passive control strategies, using the piezoelectric resonant shunt device, have been tested on this natural frequency. Frequency responses of the structure in still water are measured using two of the transducers to provide the excitation of the structure, which allow non-contact excitation and measurement. With this methodology, it is possible to

determine the parameters required for the shunt design (natural frequencies in open circuit and coupling factors). Then, the control solution is tested in still air and water. Again, for incremental difficulty, the inductor is first realized using a semi-passive method *via* a synthetic inductor. Comparisons of the in-air and in-water coupling factors give an important result relative to the expected performances of a resonant piezoelectric shunt in water. Indeed, as the coupling factors are similar, the performances of the control solution will also be similar for comparable damping coefficients. This first result may increase the confidence in the potential of the electromechanical coupling inherent to piezoelectric materials for passive vibration damping under hydrodynamic flows.

Third, a numerical setup, based on a fluid-structure-piezoelectricity interaction, is experimentally validated to estimate the coupling factors of the submerged structure. Special care is taken to consider the influence of the soft layer thickness in the overall stiffness of the structure. Consequently, it is a very valuable tool to study different positioning of the transducers and determine the optimal design to maximize the coupling factors.

Finally, vibration damping of the structure under various hydrodynamic flows, characterized by a significant reduction of the RMS value, is obtained with the semi-passive method, which represents, to the best of the authors' knowledge, the first experimental demonstration.

Additional work is currently undergoing for i) use of a purely passive inductor, custom-built to exhibit high-inductance values, ii) design of a new prototype (using the numerical model) with different transducers types and positioning to control the first torsional mode in lock-in with the von Kármán vortex-shedding, leading to the most extreme vibrations and iii) consideration of a more realistic geometry of a hydrofoil with a leading edge and a truncated trailing-edge.

Acknowledgements

The authors thanks the Arts Carnot Institute (IC ARTS) for its financial support on the project Smart Lifting Surfaces. The authors would also like to extend their warmest thanks to Jean-Michel Perron and Alain Boulch (IRENav) and to Frédéric Guillerm (LMSSC), for their extensive contributions to the experimental testing.

References

[1] M.C. Reese, Vibration and damping of hydrofoils in uniform flow, The Pennsylvania University, 2010.
[2] A. Lelong, P. Guiffant, J.-A. Astolfi, An Experimental Analysis of the Structural Response of Flexible Lightweight Hydrofoils in Cavitating Flow, J. Fluids Eng. 2:021116 (2017).
[3] J. Carlton, Marine Propellers and Propulsion, 2nd ed., Elsevier, 2007.
[4] W.F. Baker, D.S. Korista, L.C. Novak, Burj Dubai: Engineering the world's tallest building, Struct. Des. Tall Spec. Build. 16 (2007) 361–375. https://doi.org/10.1002/tal.418.
[5] E. Naudascher, D. Rockwell, Flow-Induced Vibrations: An Engineering Guide, Dover Publ, 2005.
[6] W.K. Blake, Excitation of Plates and Hydrofoils by Trailing Edge Flows, J. Vib. Acoust. Stress. Reliab. Des. 106 (1984) 351–363. https://doi.org/10.1115/1.3269201.
[7] P. Ausoni, Turbulent Vortex Shedding from a Blunt Trailing Edge Hydrofoil, Ecole Polytechnique Fédérale de Lausanne, 2009.
[8] R.S.. Moheimani, A.J. Fleming, Piezoelectric Transducers for Vibration Control and Damping, Springer-Verlag London Ltd, 2006.
[9] A. Deraemaeker, H. Nasser, A. Benjeddou, A. Preumont, Mixing Rules for the Piezoelectric Properties of Macro Fiber Composites, J. Intell. Mater. Syst. Struct. 20 (2009) 1475–1482. https://doi.org/10.1177/1045389X09335615.
[10] F. Bachmann, P. Ermanni, Integration of encapsulated piezoelectric actuators in highly loaded CFRP structures., in: Act. Passiv. Smart Struct. Integr. Syst. 2010., 2010.
[11] A. Presas, Y. Luo, Z. Wang, D. Valentin, M. Egusquiza, A review of pzt patches applications in submerged systems, Sensors (Switzerland). 18 (2018). https://doi.org/10.3390/s18072251.
[12] A. Baz, S. Poh, Performance of an active control system with piezoelectric actuators., J. Sound Vib. 126 (1988) 327–343.
[13] S. Narayanan, V. Balamurugan, Finite element modelling of piezolaminated smart structures for active vibration control with distributed sensors and actuators., J. Sound Vib. 262 (2003) 529–562.
[14] M.K. Kwak, D.H. Yang, Dynamic modelling and active vibration control of a submerged rectangular plate equipped with piezoelectric sensors and actuators, J. Fluids Struct. 54 (2015) 848–867. https://doi.org/10.1016/j.jfluidstructs.2015.02.001.
[15] S. Li, D. Zhao, Numerical simulation of active control of structural vibration and acoustic radiation of a fluid-loaded laminated plate., J. Sound Vib. 272 (2004) 109–124.
[16] S. Li, Active modal control simulation of vibro-acoustic response of a fluid-loaded plate., J. Sound Vib. 330 (2011) 5545–5557.
[17] N.W. Hagood, A. von Flotow, Damping of Structural Vibrations with Piezoelectric Materials and Passive Electrical Networks, J. Sound Vib. 146 (1991) 243–268. https://doi.org/10.1049/em:19910037.
[18] O. Thomas, J. Ducarne, J.-F. Deü, Performance of piezoelectric shunts for vibration reduction, Smart Mater. Struct. 21 (2012). https://doi.org/10.1088/0964-1726/21/1/015008.
[19] J. Ducarne, O. Thomas, J.F. Deü, Placement and dimension optimization of shunted piezoelectric patches for vibration reduction, J. Sound Vib. 331 (2012) 3286–3303. https://doi.org/10.1016/j.jsv.2012.03.002.
[20] K. Yamada, Complete passive vibration suppression using multi-layered piezoelectric element, inductor, and resistor, J. Sound Vib. 387 (2017) 16–35. https://doi.org/10.1016/j.jsv.2016.10.009.

[21] H. He, X. Tan, J. He, F. Zhang, G. Chen, A novel ring-shaped vibration damper based on piezoelectric shunt damping: Theoretical analysis and experiments, J. Sound Vib. 468 (2020) 115125. https://doi.org/10.1016/j.jsv.2019.115125.

[22] M. Berardengo, O. Thomas, C. Giraud-audine, M. Berardengo, O. Thomas, C. Giraud-audine, S. Manzoni, Improved resistive shunt by means of negative capacitance : new circuit , performances and multi-mode control, Smart Mater. Struct. 25 (2016).

[23] B. Lossouarn, J.F. Deü, M. Aucejo, Multimodal vibration damping of a beam with a periodic array of piezoelectric patches connected to a passive electrical network, Smart Mater. Struct. 24 (2015). https://doi.org/10.1088/0964-1726/24/11/115037.

[24] B. Lossouarn, M. Aucejo, J. Deü, B. Multon, Physical Design of inductors with high inductance values for resonant piezoelectric damping, Sensors Actuators A. Phys. 259 (2017) 68–76. https://doi.org/10.1016/j.sna.2017.03.030.

[25] J.F. Toftekær, J. Høgsberg, Experimental validation of piezoelectric shunt tuning with residual mode correction: Damping of plate-like structures, J. Intell. Mater. Syst. Struct. 31 (2020) 1220–1239. https://doi.org/10.1177/1045389X20914393.

[26] J.M. Zhang, W. Chang, V.K. Varadan, V. V. Varadan, Passive underwater acoustic damping using shunted piezoelectric coatings, Smart Mater. Struct. 10 (2001) 414–420. https://doi.org/10.1088/0964-1726/10/2/404.

[27] Y. Sun, Z. Li, A. Huang, Q. Li, Semi-active control of piezoelectric coating's underwater sound absorption by combining design of the shunt impedances., J. Sound Vib. 355 (2015) 19–38.

[28] C. Li, E.J. Chae, Y.L. Young, X. Wang, S. Alben, Passive Vibration Control of Flexible Hydrofoils Using Piezoelectric Material, in: Fourth Int. Symp. Mar. Propulsors Smp'15, Austin, Texas, USA, June 2015, 2015.

[29] O.D. La Torre, X. Escaler, E. Egusquiza, M. Farhat, Experimental investigation of added mass effects on a hydrofoil under cavitation conditions, J. Fluids Struct. 39 (2013) 173–187. https://doi.org/10.1016/j.jfluidstructs.2013.01.008.

[30] L. Pernod, A. Ducoin, H. Le Sourne, J.-A. Astolfi, P. Casari, Experimental and numerical investigation of the fluid-structure interaction on a flexible composite hydrofoil under viscous flows, Ocean Eng. 194 (2019). https://doi.org/10.1016/j.oceaneng.2019.106647.

[31] V. Strouhal, Über eine Besondere Art der Tonerzeugung (Special Kind of the Tone Generation), Ann. Phys. 241 (1878).

[32] A. Mallock, On the resistance of air., Proc. R. Soc. London Ser. A. 79 (1907) 262–265.

[33] H. Bénard, Formation de centres de giration à l'arrière d'un obstacle en mouvement., Comptes Rendus l'Académie Des Sci. Paris. 147 (1908) 839–842.

[34] A. Zobeiri, Effect of Hydrofoil Trailing Edge Geometry on the Wake Dynamics, EPFL (Ecole Polytechnique Fédérale de Lausanne), 2012. https://doi.org/10.5075/epfl-thesis-5218.

[35] A. Mehmood, A. Abdelkefi, M.R. Hajj, A.H. Nayfeh, I. Akhtar, A.O. Nuhait, Piezoelectric energy harvesting from vortex-induced vibrations of circular cylinder, J. Sound Vib. 332 (2013) 4656–4667. https://doi.org/10.1016/j.jsv.2013.03.033.

[36] A. Presas, D. Valentin, E. Egusquiza, C. Valero, M. Egusquiza, M. Bossio, Accurate determination of the frequency response function of submerged and confined structures by using PZT-patches, Sensors (Switzerland). 17 (2017). https://doi.org/10.3390/s17030660.

[37] Z. Yao, F. Wang, M. Dreyer, M. Farhat, Effect of trailing edge shape on hydrodynamic damping for a hydrofoil, J. Fluids Struct. 51 (2014) 189–198. https://doi.org/10.1016/j.jfluidstructs.2014.09.003.

[38] C. Seeley, A. Coutu, C. Monette, B. Nennemann, H. Marmont, Characterization of hydrofoil damping due to fluid-structure interaction using piezocomposite actuators, Smart Mater. Struct. 21 (2012). https://doi.org/10.1088/0964-1726/21/3/035027.

[39] A. Preumont, B. de Marneffe, A. Deraemaeker, F. Bossens, The damping of a truss structure with a piezoelectric transducer, Comput. Struct. 86 (2008) 227–239. https://doi.org/10.1016/j.compstruc.2007.01.038.

[40] E. De Langre, Fluides et solides, 1st ed., Palaiseau : Editions de l'Ecole Polytechnique, 2002. http://books.google.com/books?hl=en&lr=&id=IFnLwQ4eTIwC&oi=fnd&pg=PA13&dq=Fluides+et+solides&ots=OCy2qgK6xQ&sig=zqJNYyWNOKq0F2ytut4lHFYBkGg.

[41] K. Dekemele, P. van Torre, M. Loccufier, High Voltage Synthetic Inductor in Piezoelectric Shunt to Damp Flexible Vibrating Structures, in: IX ECCOMAS Themat. Conf. Smart Struct. Mater., 2019: pp. 922–929.

[42] J.F. Deü, W. Larbi, R. Ohayon, R. Sampaio, Piezoelectric shunt vibration damping of structural-acoustic systems: Finite element formulation and reduced-order model, J. Vib. Acoust. Trans. ASME. 136 (2014). https://doi.org/10.1115/1.4027133.

[43] Blake, Maga, Finkelstein, Hydroelastic Variables Influencing Propeller and Hydrofoil Singing, in: Noise Fluids Eng. Proc. Winter Annu. Meet. Am. Soc. Mech. Eng., 1977.